e-mail: christoph.naegerl@uibk.ac.at

Key words Bose-Einstein condensation

Appl.Phys.B manuscript No.
(will be inserted by the editor)

Optimized production of a cesium Bose-Einstein condensate

Tobias Kraemer[1], Jens Herbig[1], Michael Mark[1], Tino Weber[1], Cheng Chin[1], Hanns-Christoph Nägerl[1⋆], and Rudolf Grimm[1,2]

[1]Institut für Experimentalphysik, Universität Innsbruck, Technikerstraße 25, A-6020 Innsbruck, Austria
[2]Institut für Quantenoptik und Quanteninformation, Österreichische Akademie der Wissenschaften, A-6020 Innsbruck, Austria

Received: date / Revised version: date

Abstract We report on the optimized production of a Bose-Einstein condensate of cesium atoms using an optical trapping approach. Based on an improved trap loading and evaporation scheme we obtain more than 10^5 atoms in the condensed phase. To test the tunability of the interaction in the condensate we study the expansion of the condensate as a function of scattering length. We further excite strong oscillations of the trapped condensate by rapidly varying the interaction strength.

PACS: 03.75.Kk; 32.80.Pj

1 Introduction

Much of the present work in the field of quantum gases relies on optical trapping techniques and on the ability to tune atomic interactions. Optical approaches have been recently employed in several atomic Bose-Einstein condensation experiments [1,2,3,4,5] and in experiments on the production of ultracold molecular samples [6,7,8,9,10] and on molecular Bose-Einstein condensates [11,12]. The major advantages in optical traps are the possibility to trap atoms in any sublevel of the electronic ground state and the ease to adjust the interaction strength using magnetically induced Feshbach resonances.

The cesium atom is very attractive for experiments with tunable atomic interactions. The lowest internal quantum state of Cs features a unique combination of wide and narrow Feshbach resonances which are easily accessible at low magnetic fields [13]. This results in a great flexibility for tuning the atomic scattering properties. In particular, magnetic tuning of the interaction strength has recently allowed the first realization of a Bose-Einstein condensate (BEC) with Cs atoms [4] and the realization of a two-dimensional condensate very close to a dielectric surface [5]. The tunability of the atomic interaction can be exploited in experiments where one might wish to adjust or to dynamically change the mean-field interaction of the condensate. Also, the Feshbach resonances can be used to produce molecules from an atomic BEC [14,8,9,10] and to study the transition from an atomic BEC to a molecular BEC. In this context, a quantum phase transition with an essentially topological character has been predicted [15,16]. For such and many other intriguing experiments it is desirable to have a large BEC of Cs atoms as a starting point.

In this paper we report on the optimized production of an essentially pure Cs BEC in the lowest internal quantum state with more than 10^5 atoms. Since this state cannot be trapped by purely magnetic means, the path to condensation relies on a sequence of optical traps. We discuss the loading and transfer from one trap to the next and give a detailed description of the evaporation path and of the resulting condensate. As a demonstration for tunability we measure the expansion energy as a function of scattering length in time-of-flight experiments. In particular, we show the ultra-slow expansion of the condensate after release from the trap for nearly vanishing scattering length. The release energy corresponds to ~ 50 pK. Finally, we present first results when the scattering length is suddenly stepped and the condensate then starts to oscillate freely in the trap.

2 Cesium scattering properties and Feshbach resonances

Early experiments [17,18] towards condensation of cesium focused on samples in magnetic traps polarized either in the upper hyperfine ground state $F = 4$, magnetic sublevel $m_F = 4$, or in the lower hyperfine state $F = 3, m_F = -3$. Here, F denotes the total angular momentum and m_F the magnetic quantum number. The spin relaxation rates were measured to be several orders of magnitude higher than expected [19,20,21]. It was later understood that this is caused by the dipolar relaxation process induced by the second-order spin-orbit interaction [22]. The maximum phase-space density in a small sample of Cs atoms was a factor of about four away from condensation [23].

The problem of the strong inelastic two-body losses can be overcome by using the lowest internal state of cesium,

⋆ corresponding author

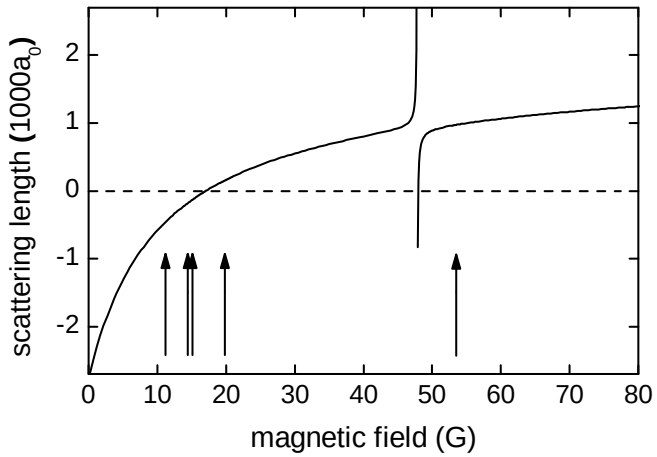

Fig. 1 Scattering length as a function of magnetic field for the state $F = 3, m_F = 3$. There is a relatively broad Feshbach resonance at 48.0 G due to coupling to a d-wave molecular state. The arrows indicate several very narrow resonances at 11.0, 14.4, 15.0, 19.9 and 53.5 G, which result from coupling to g-wave molecular states. The data is taken from [13].

$F = 3, m_F = 3$ [24,25,26,27]. In this state, all inelastic two-body processes are endothermic and are thus fully suppressed at sufficiently low temperature. This state requires optical trapping since it cannot be captured in a magnetic trap. Optically trapped atoms can only be efficiently evaporated by lowering the total potential depth. This process weakens the confinement of the trapped sample and thus makes it difficult to achieve sufficiently high elastic collision rates for effective evaporation. Hence, adjustability of the collisional properties is very helpful for a fast evaporation strategy.

The success in condensing Cs [4] largely relies on the fact that the s-wave scattering length for the $F = 3, m_F = 3$ state can be tuned to moderate and positive values by the application of relatively low dc magnetic fields [13]. As Fig. 1 shows, an external magnetic field allows for precise tuning of the atomic scattering length a from negative to positive values. Positive scattering lengths in the range between zero and one thousand a_0 are attained for magnetic fields of a few ten Gauss; a_0 denotes Bohr's radius. In particular, there is a gentle zero-crossing of the scattering length near 17 G [25]. Here, the interaction of atoms in a BEC is effectively switched off. Several narrow higher-order Feshbach resonances [13], caused by coupling to d- and g-wave molecular states, enable very rapid control of the atomic scattering properties. With the magnetic field being a free parameter in our optical trapping approach, we can take full advantage of this tunability of the s-wave scattering length.

For Cs in the $F = 3, m_F = 3$ ground state the process of three-body recombination is the dominant loss and heating mechanism [28]. In a recombination process, three atoms collide, two of them form a molecule, and the third atom takes away two thirds of the binding energy according to energy and momentum conservation. The atoms that form the molecule are usually lost, and the third atom is either lost or it deposits its share of the binding energy in the sample. Heating of the sample is the combination of "anti-evaporation" and recombination heating [28]. To a good approximation, the three-body recombination rate scales with the fourth power of the scattering length. Unfortunately, the prefactor in this scaling law is measured to be relatively large [28]. To minimize this heating, the recombination products should be removed quickly from the trap. It is thus important to assure that the sample is not operated too deep in the hydrodynamic regime and that the evaporation is efficient in *all* directions. Arbitrarily increasing the scattering length to speed up the forced evaporation is therefore not possible without sacrificing cooling efficiency. Within these limits, tuning the scattering length allows for an optimization of the evaporation for given trap parameters. For example, for the low initial densities in a large reservoir trap the evaporation may be sped up by increasing the scattering length. In a later trapping stage with a higher atomic density the scattering length should be reduced to optimize the ratio of good to bad collisions.

3 BEC production

3.1 Overview of experimental strategy

For producing large condensates in optical dipole traps, it is necessary to independently optimize both trap loading and evaporative cooling. For initial loading of as many atoms as possible, an optical trap with large volume is needed which, in view of limited laser power, implies a shallow trapping potential. For subsequent forced evaporative cooling, however, high densities and fast elastic collisions require much tighter confinement. These two requirements in general demand dynamical changes of the trapping potential. A possible way to implement this is a spatial compression of the optical trap using e.g. a zoom-lens system [29]. Our approach is based on an alternative way where a sequence of optical trapping schemes is used to provide optimized loading together with optimized evaporative cooling.

We first use a shallow, large volume CO_2-laser trap as a "reservoir" for collecting the atoms before forced evaporative cooling is implemented in a tighter trap. The reservoir trap can be efficiently loaded with atoms that are precooled by Raman-sideband cooling [30]. This approach allows collection of atoms at moderate densities with little loss from three-body collisions and with negligible heating from either photon scattering or trap vibrations. It serves as a good starting point for the final transfer into a tighter optical trap. The tighter trap is adiabatically increased and adds a "dimple" to the trapping potential of the reservoir. Collisional loading of this dimple already yields a significant enhancement of the local number and phase-space density [31]. After turn-

ing off the reservoir trap excellent conditions for further forced evaporative cooling are obtained.

The different trap stages of optical trapping used in our experiments are illustrated in Fig. 2. An overview of the evolution of phase-space density and particle number for the various trapping stages is shown in Fig. 3.

The use of relatively weak optical trapping necessitates the implementation of magnetic "levitation" where a magnetic field gradient along the vertical direction compensates for the gravitational force. This levitation turns out to be very useful in two ways: First, in the limit of very weak optical trapping only one spin state is held in the trap. This assures perfect spin polarization of the sample[1]. Further, efficient evaporation can be performed without the effect of gravitational sag in the trap. The dc magnetic field offset remains a free parameter for flexible tuning of the scattering length.

3.2 Laser cooling

The initial collection and cooling of Cs atoms is achieved by conventional techniques. In a stainless steel vacuum chamber [32] atoms are loaded into a magneto-optical trap (MOT) from a Zeeman slowed atomic beam with up to 3×10^8 atoms after about 6 s. The MOT is operated on the $6^2S_{1/2}, F = 4$ to $6^2P_{3/2}, F' = 5$ transition. The ultra-high vacuum of less than 1×10^{-11} mbar gives 200 s for the $1/e$-lifetime of the MOT. The MOT light is derived from a high power laser diode[2] referenced via beat-lock to a grating-stabilized master diode laser. Standard absorption imaging is used to determine particle numbers and temperatures.

We compress the atomic cloud by ramping up the magnetic field gradient in the MOT by a factor of 5 to 33 G/cm within 40 ms. Simultaneously we linearly change the detuning of the MOT laser from around 10 MHz to 30 MHz. At the end of the ramp, we switch off the MOT light and the magnetic field gradient. To cool the compressed cloud, we then apply degenerate Raman-sideband cooling [30] in an optical lattice to further cool and to polarize the atoms in the desired $F = 3, m_F = 3$ state. We have adapted the technique as described in [33] to our setup. This cooling scheme is particularly suited for polarizing atoms in the $F = 3, m_F = 3$ state because this is a dark state for which photon scattering is suppressed. Four laser beams derived from an injection locked slave laser resonant with the $F = 4$ to $F' = 4$ transition produce a three-dimensional optical lattice, drive Raman-sideband transitions and repump out of the $F = 4$ ground state manifold. The total power of all the four beams is 65 mW and their $1/e^2$-beam radii are about 1 mm. The oscillation frequency in the lattice is on the order of 100 kHz. A small magnetic field offset of several hundred mG is applied to induce the Raman-sideband cooling. We succeed in polarizing 90% of the atoms. The ensemble is then adiabatically released from the lattice after 6 ms of cooling time. If the atomic cloud is released into free space, the temperature of the ensemble with up to 4×10^7 atoms is about $0.7\,\mu$K. For our typical atomic densities this corresponds to a phase space density of 1×10^{-3}.

3.3 Reservoir trap

We generate the large reservoir trap by horizontally crossing two CO_2-laser beams A_1 and A_2 at right angles as shown in Fig. 2(a). At the same time we apply a magnetic gradient field in the vertical direction to levitate the atoms against gravity. The delivered powers in laser beams A_1 and A_2 are 90 W and 65 W, respectively. The light comes from two separate, highly stable linearly polarized single-frequency CO_2-lasers[3]. Switching of the beams is done by external acousto-optical modulators[4] (AOMs). A_1 is downshifted in frequency by 40 MHz, whereas A_2 is upshifted by 40 MHz to prevent any interference. To avoid mode-hops the cooling water for the lasers needs to be stabilized to better than ± 20 mK. Still, a slow mode drift changes the power of the lasers by a few percent over the time scale of minutes. At the crossing point the $1/e^2$-beam radii of the two lasers are $(605 \pm 35)\,\mu$m and $(690 \pm 35)\,\mu$m.

The magnetic fields for levitation and for Feshbach tuning are generated by two pairs of coils aligned with their axes parallel to the vertical direction. One pair in anti-Helmholtz configuration produces the vertical magnetic field gradient near 31.3 G/cm to levitate the atoms in the $F = 3, m_F = 3$ state. Another pair in Helmholtz configuration provides a variable bias field B_0 of up to 200 G. The combined field results in a weak outward directed force $F(\rho) = m\alpha^2\rho$ depending on the horizontal distance ρ from the vertical symmetry axis. For perfect levitation of our atoms the constant $\alpha = g\sqrt{m/(3\mu_B B_0)}$ describes the curvature of the parabolic anti-trapping potential. The levitation field thus slightly reduces the trap depth along the horizontal direction. Here, m is the mass of Cs, g is the gravitational acceleration, and μ_B is Bohr's magneton. At $B_0 = 17$ G we have $\alpha = 2\pi \times 3.4$ Hz. The horizontal trap frequencies $\omega_{x,y}$ are reduced according to $\omega'_{x,y} = \sqrt{\omega^2_{x,y} - \alpha^2}$. This is usually a very small effect for all but the lowest trap frequencies. Note that levitation also affects the horizontal motion of free atoms after the optical trap is shut off. The horizontal motion follows $\rho(t) = \rho_0 \cosh(\alpha t) + \alpha^{-1} v_0 \sinh(\alpha t)$ for initial position ρ_0 and initial velocity v_0. The vertical motion is not affected.

We excite vertical trap oscillations by briefly changing the vertical magnetic field gradient and hence tilting the trap. For exciting horizontal trap oscillations we shift the equilibrium position of the atoms by adding a horizontal magnetic field component. In both cases we monitor the center-of-mass oscillation of the atomic cloud after 50 ms time-of-flight. The geometrically averaged trap frequency $\bar{\nu}$ is calculated to be (12.6 ± 1.5) Hz which is in good agreement with the experimental value of (13.2 ± 0.2) Hz. Together with the levitation and the magnetic bias field the lasers provide an effective trap

[1] This Stern-Gerlach separation technique also allows for radio-frequency evaporation along the vertical direction. Al-

[3] Coherent-DEOS GEM-100L

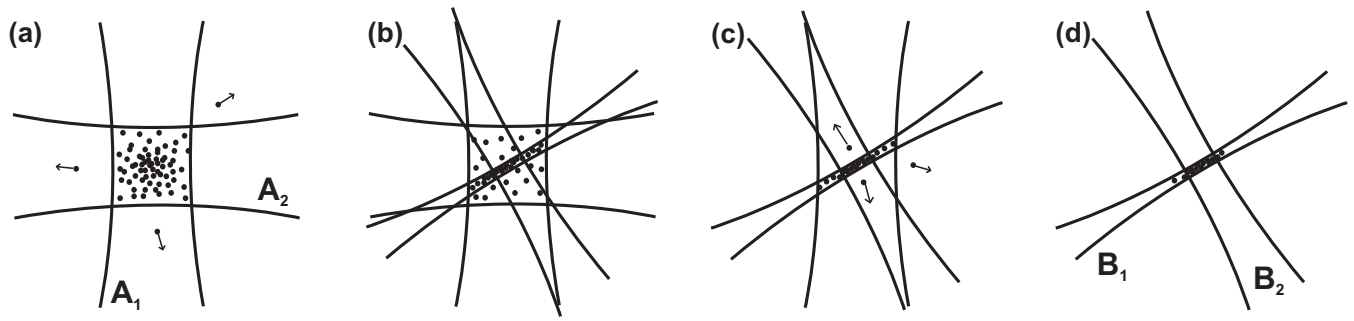

Fig. 2 Illustration of the various stages of trap loading and evaporative cooling as seen from above. (a) Plain evaporation in a crossed CO_2-laser trap generated by beams A_1 and A_2 at a scattering length of $a = 1215\,a_0$. (b) 1.5 s of ramping and collisional loading into a crossed 1064-nm fibre laser trap generated by beams B_1 and B_2 with a final scattering length $a = 210\,a_0$. (c) Forced evaporative cooling after switching off CO_2-laser beam A_2. The power of all remaining lasers is ramped down, and the power in CO_2-laser beam A_1 is reduced to zero. (d) Final configuration of the crossed 1064-nm trap. Imaging is done in the horizontal plane at an angle of 30° with respect to the long axis of the cigar-shaped atomic cloud.

depth of about $k_B \times 7\,\mu$K. This trap depth is given by the weaker of the two CO_2-lasers as the atoms can escape along the direction of the stronger beam.

For transfer of the precooled atoms into the reservoir trap, we leave the light of the two CO_2-lasers on during the entire pre-cooling phase. This is because the CO_2-lasers show strong variations in beam pointing and beam shape as a function of radio-frequency power to the AOMs. We have checked that the small light shift introduced by the lasers does not affect the initial loading and cooling efficiency. The reservoir trap is then activated by ramping up the magnetic field and its gradient. The $1/e$-rise time of the magnetic fields is limited to 1.5 ms because of eddy currents in the stainless steel chamber. We therefore do not expect the transfer to be fully adiabatic.

We find that the atoms are heated to about $2.2\,\mu$K by the transfer into the reservoir trap. A clear measurement on the trapped sample is only possible after about 50 ms since the system initially is not in thermal equilibrium and since the untrapped atoms need to disappear from the field of view. We largely attribute the heating to imperfect phase space matching. In fact, the atomic cloud after Raman-sideband cooling to $0.7\,\mu$K has a $1/e$-radius of $\sim 350\,\mu$m. In comparison, an equilibrium distribution in the reservoir trap at $0.7\,\mu$K would have a $1/e$-radius of $\sim 100\,\mu$m. Potential energy is thus gained which is then turned into kinetic energy, effectively heating the cloud of atoms. Subsequently, the hot atoms evaporate out of the trap. For this phase of plain evaporation we set the magnetic bias field to 73.5 G. The scattering length is then $1215\,a_0$. The temperature is reduced to less than $1\,\mu$K within 10 s. After this time, we measure more than 4×10^6 atoms, corresponding to a peak phase space density of 2×10^{-3}.

3.4 Dimple trap

We proceed with loading of the dimple trap after 2 s of plain evaporation in the reservoir trap. At this point the atom number is 7.8×10^6 and the phase space density is 1.7×10^{-3} (see Fig. 3). The dimple trap is generated by horizontally intersecting one tightly focused laser beam B_1 with 34-μm waist and another less focused beam B_2 with 260-μm waist at right angles, rotated by 30° in the horizontal plane with respect to the CO_2-laser beams as shown in Fig. 2(d). This is different from our earlier work [4] where we have used CO_2-laser beam A_2 for axial confinement. We introduce the B_2 beam because some weak back reflections of the CO_2-laser beams led to a slight undesirable corrugation of the optical potential. This complicated the quantitative analysis of the BEC. Beams B_1 and B_2 are derived from a broadband fiber laser[5] at 1064 nm. The powers in these beams are ramped up within 1.5 s to a maximum power of 70 mW for B_1 and 270 mW for B_2. The trapping in the dimple is now briefly done by all four laser beams with B_1 providing most of the radial and A_1 most of the axial confinement. After switching off beam A_2 we measure the radial and axial trap frequencies in the dimple to (221.2 ± 1.6) Hz and (14.2 ± 0.1) Hz, respectively. During the ramping up phase of B_1 and B_2 we reduce the magnetic field offset to 23 G and thus the scattering length to $300\,a_0$ in order to reduce losses from three-body recombination [28]. The trap now contains about 1.7×10^6 atoms at a peak phase space density of approximately 0.13.

3.5 Forced evaporation towards BEC

We start forced evaporative cooling by ramping down the power in all three remaining beams. Simultaneously we remove the reservoir by switching off the CO_2-laser A_2 that is not responsible for axial confinement. To assure a well-defined ramp over a large intensity range we control the light power of the near-infrared beam B_1 by means of a logarithmic photodiode and a servo loop. The power in CO_2-laser beam A_1 is ramped to zero within 5.5 s so that B_2 at the end of evaporation exclusively assures axial confinement. The change in beam pointing for A_2 does not affect the evaporation. For B_1 we approxi-

[5] IPG Laser PYL-10

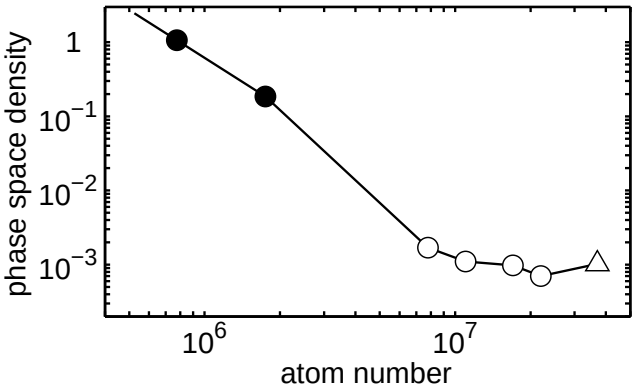

Fig. 3 Peak phase space density as function of atom number. The path of evaporation proceeds from right to left. The *triangle* shows the atomic ensemble immediately after lattice cooling. The *open circles* show the ensemble in the reservoir trap after 0.08, 0.22, 0.64, and 2.0 s. The *filled circles* correspond to the sample in dimple trap right after loading and after 1.5 s of evaporation. The phase transition occurs after 2 s of forced evaporation with $\sim 5 \times 10^5$ atoms left in the dimple trap.

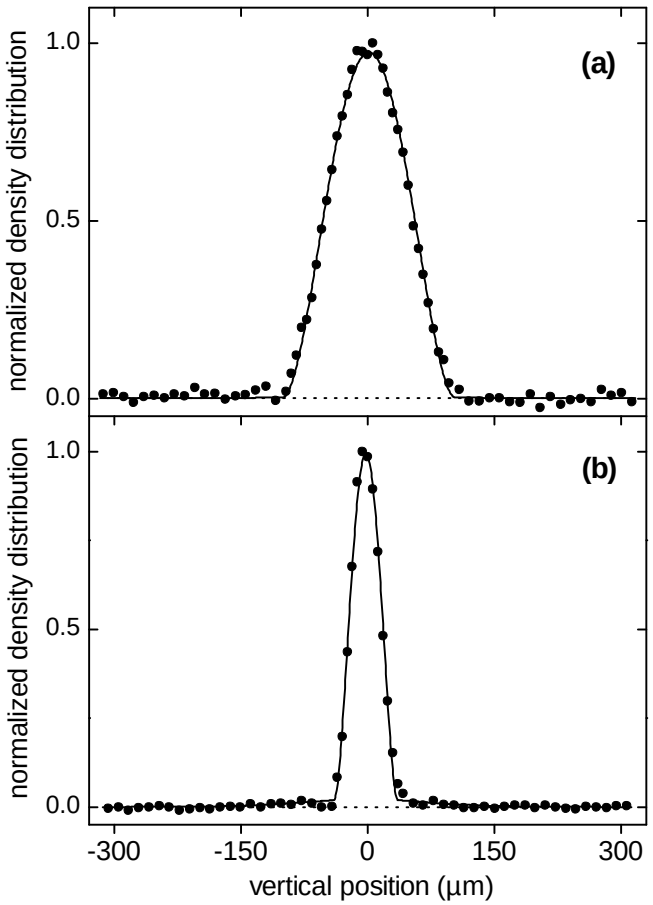

Fig. 4 Vertical density profiles of Cs condensates after 100 ms of free expansion in the levitation field. The solid curves are fits to the data for the Thomas-Fermi profiles which include possible thermal components. For better distinction the baseline is dashed. (a) Expansion with no change in scattering length. The total number of atoms in the condensate is $N = 1.1 \times 10^5$. (b) Expansion near zero scattering length under the same conditions reveals a small thermal component with a temperature of about 10 nK.

mately follow an exponential ramp over 5.5 s. The power in beam B_2 is only slightly reduced. The final power in B_1 and B_2 is 0.5 mW and 220 mW. We find and optimize this ramp by extending the ramp in discrete time steps of a few hundred milliseconds at the beginning and up to one second towards the end of the ramp.

At each step we search for a maximum in evaporation efficiency $\gamma = \log(D'/D)/\log(N/N')$ as a function of the trap depth and scattering length [34]. Here, D and D' are the phase-space densities at the beginning and end of each step, N and N' denote the respective particle numbers. Maximizing γ at each step results in an overall optimization of the evaporation path. We find that a magnetic field value of 21 G with scattering length $a = 210\,a_0$ is optimal during the forced evaporation phase. As can be seen from Fig. 3 the efficiency γ lies around 3 during the forced evaporation ramp. We attribute this high efficiency to the fact that atoms can escape the trap into almost all directions because of the levitation field. We observe the phase transition after 2 s of forced evaporative cooling with about 5×10^5 atoms at a temperature of (200 ± 10) nK. At this point the power in beams B_1 and B_2 is 8.7 mW and 250 mW. The duration of the ramp is relatively short. Our evaporation proceeds close to the hydrodynamic regime. Thus, significant improvement of the evaporation is not to be expected.

Further evaporation leaves a cigar-shaped condensate with the long axis in the horizontal plane. In Fig. 4 we show vertical density profiles of expanding condensates. The tunability of the scattering length allows us to explore different regimes of expansion. For Fig. 4(a) we expand the condensate at the creation scattering length of $210\,a_0$. This is the usual type of self-similar expansion in which the condensate in the Thomas-Fermi regime retains its parabolic shape [35]. For Fig. 4(b) we step the scattering length to zero at the moment of release from the trap. The mean-field interaction thus vanishes and the rate of expansion is greatly reduced. This exposes a small thermal component, for which a bimodal fit reveals a temperature of around 10 nK. The critical temperature at these trapping conditions is 24 nK, therefore the expected condensate fraction agrees well with the measured value of 91%. From the fit to the data in Fig. 4 we obtain that there are up to 1.1×10^5 atoms in the condensate with a 20% calibration error. The error does not come from the fit but from the overall uncertainty in determining the atom number. Usually, the error from absorption imaging alone is around 50%, but we can calibrate the atom number from measurements on the chemical potential, see Sec. 4.1. For this particular experiment we measure the final trap frequencies to (4.3 ± 0.2) Hz

and (21.1 ± 0.2) Hz along the axial and radial direction, respectively. We thus infer for the initial Thomas-Fermi sizes $R_r^{TF} = (8.7 \pm 0.3)\,\mu$m and $R_a^{TF} = (42.5 \pm 1.2)\,\mu$m along the radial and axial directions at a scattering length of $a = 210\,a_0$. The peak density of the condensate is $n_0 = (2.1 \pm 0.1) \times 10^{13}$ cm^{-3}.

4 Tunable quantum gas

We now test the tunability of the condensate interaction. We first study the condensate expansion as a function of scattering length [36] in two different ways. We then specialize to the case when the interaction energy is switched off and present improved results on the ultra-slow expansion of the condensate in comparison with earlier measurements in [4]. Finally, we excite compression oscillations of the trapped condensate by suddenly stepping the scattering length to a lower value.

4.1 Expansion energy as a function of scattering length

We measure the release energy of the condensate for slow and fast changes of the scattering length. When we slowly vary the scattering length the wave function of the trapped condensate can follow adiabatically and the condensate remains in equilibrium. The release energy is proportional to the chemical potential of the condensate at the given value of the scattering length. The situation is different when we rapidly switch the scattering length at the moment of condensate release. The condensate then expands from a non-equilibrium state because the wave function has not had time to adjust to the change in interaction energy. This leads to strong changes for the rate of condensate expansion in comparison to the expansion from equilibrium.

We first consider a condensate in the Thomas-Fermi regime for which we adiabatically ramp the scattering length to a new value. For such a condensate, the release energy E_{rel} directly corresponds to the chemical potential μ_{TF} through $\frac{7}{2}E_{rel} = \mu_{TF}$ [35], which is given by

$$\mu_{TF} = \frac{h\,\bar{\nu}}{2}\left(\frac{15\,N}{a_{ho}}\right)^{2/5} a^{2/5}. \qquad (1)$$

Here, $\bar{\nu}$ is the geometric average of the trap frequencies, N is the particle number in the condensate, and $a_{ho} = \sqrt{\hbar/(m\,2\pi\,\bar{\nu})}$ is the oscillator length. For the experiment we produce a condensate with $N = 8.5 \times 10^4$ atoms at a creation scattering length of $a_c = 210\,a_0$. We then slowly ramp the magnetic field to values between 20 and 35 G, setting the scattering length to a value between about 200 and $700\,a_0$. The slow ramping excludes values below the Feshbach resonance at 19.9 and above the one at 48.0 G because of strong loss[6]. The condensate is then released from the trap and we measure the release energy. The results are shown in Fig. 5. Here we assume that the magnetic field strength translates into scattering length according to Fig. 1. The data is well fit by a function of the form $C\,a^{2/5}$ according to Eq. (1). From the fit parameter C we can deduce an independent estimate of the particle number $N = (8.2 \pm 1.3) \times 10^4$. The error is dominated by the error in determining the trap frequencies.

[6] A combination of slow ramping and quick jumping at the Feshbach resonances would allow access to the full range of

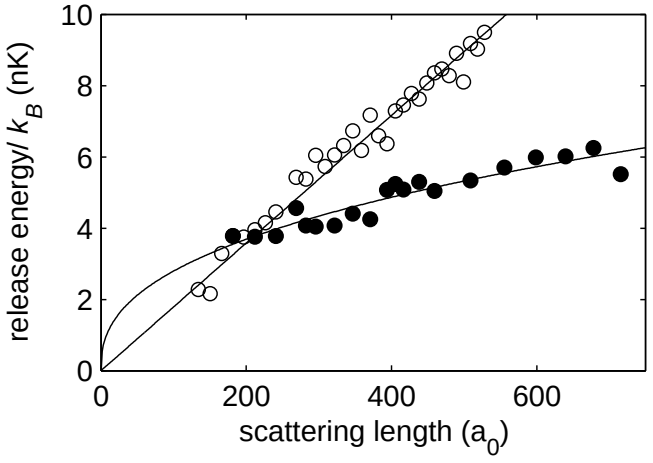

Fig. 5 Release energy of the condensate as a function of scattering length a. The *filled circles* represent experimental data for the case of adiabatic ramping of a trapped condensate. The data, corresponding to 2/7 of the chemical potential at a given value of the scattering length, is fit by $C\,a^{2/5}$. The *open circles* represent data for rapid switching at the moment of condensate release. As discussed in the text, the straight line is not a fit. It connects the origin with the fitted value of the release energy at the creation scattering length.

For a sudden change of the scattering length the condensate wave function has no time to react. For example, for an increase of the scattering length the density distribution is too narrow in comparison to the equilibrium density distribution at the new value of the scattering length. The condensate thus expands more rapidly than a condensate in equilibrium at this new value. Since the mean-field interaction energy of the condensate scales linearly with the scattering length for a given density profile [35], we expect a linear behavior of the release energy as a function of the final scattering length a. In Fig. 5 we thus compare the data for the measured release energy to a straight line $C\,a_c^{2/5}\,a/a_c$ given by the origin and the fitted value of the release energy at the creation scattering length $a_c = 210\,a_0$. We find good agreement with the linear dependence.

4.2 Ultra-slow condensate expansion

We now study the expansion of the condensate near the zero-crossing of the scattering length. At the moment of condensate release, we rapidly switch the magnetic field from the creation field near 20 G to (17.17 ± 0.05) G, corresponding to $a = (3.4 \pm 3.0)\,a_0$. The error in determining the precise magnetic field at the position of condensate requires that we choose a slightly positive value of the scattering length to assure that no weakly attractive interactions modify the condensate expansion. The levitation field remains on, allowing for an extended observation period because the atoms then do not fall under

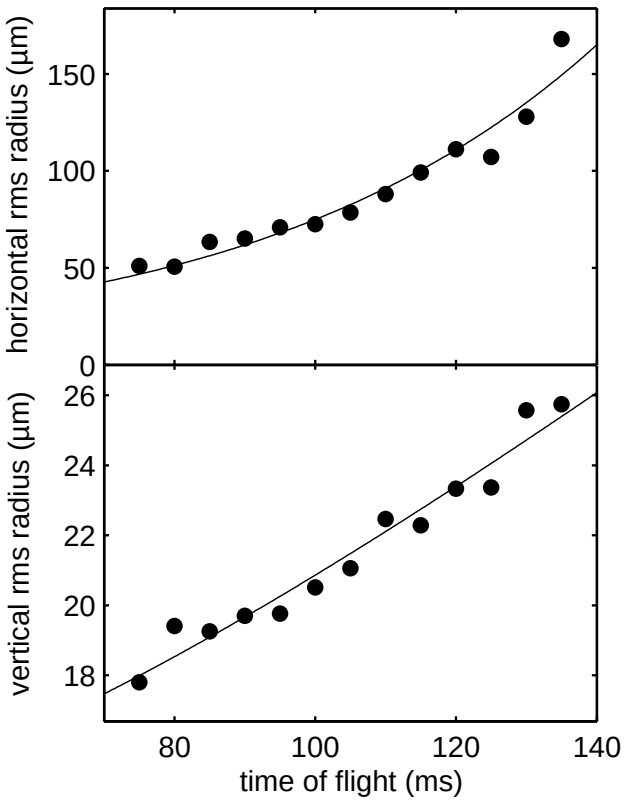

Fig. 6 Expansion of the non-interacting condensate. The data points show the horizontal (above) and vertical (below) rms radius of the BEC as a function of expansion time near the zero crossing of scattering length. Note the different scales. The fit to the residual vertical expansion reveals a release energy of $k_B \times (51 \pm 3)$ pK. For the horizontal expansion the data is fit by $A \cosh(\alpha t)$ with $\alpha = 2\pi \times (3.20 \pm 0.23)$ Hz.

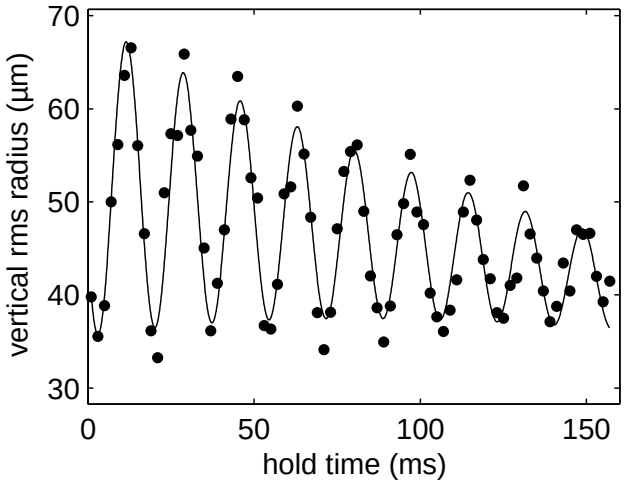

Fig. 7 Condensate oscillations after rapid switching of the scattering length. The *filled circles* show the vertical rms radius of an expanding BEC with 7×10^4 atoms after 80 ms of free expansion as a function of hold time in the trap. The scattering length has been switched rapidly from $363\,a_0$ to $25\,a_0$. The *solid curve* is a fit to the data giving an oscillation frequency of (58.3 ± 0.2) Hz. We independently measure the radial trap frequency to (28 ± 1) Hz.

gravity. Fig. 6 shows the vertical and horizontal extent of a BEC with 1.2×10^5 atoms as a function of time after release from the trap. We only show the data after 75 ms of expansion when the optical density of the atomic cloud is sufficiently reduced to allow for reliable absorption imaging. The horizontal expansion is dominated by the magnetic anti-trapping potential which derives from the presence of the levitation field and which magnifies the atomic cloud according to the cosine hyperbolicus function, see Sec. 3.3. The measured rate of expansion $2\pi \times (3.20 \pm 0.23)$ Hz agrees reasonably well with the expected rate constant $\alpha = 2\pi \times 3.4$ Hz. The vertical expansion corresponds to a release energy of $k_B \times (51 \pm 3)$ pK. Note that this is much lower than the kinetic energy of the ground state $\hbar\omega_r/4 = k_B \times 253$ pK given by a radial trap frequency of $\omega_r = 2\pi \times 21.1$ Hz. It is remarkable that the release energy is less than the zero-point energy of the ground state. Since the spatial extent of the condensate is much larger than the size of the ground state wave function of the harmonic oscillator, the momentum spread, limited by the uncertainty of the wave function of the initial condensate, is lower than that of the ground state.

4.3 Condensate oscillations

By rapidly ramping the scattering length it is possible to excite oscillations of the condensate in the trap [37]. In fact, in the limit of a cigar shaped condensate one expects radial "compression" or "expansion oscillations" at twice the trap frequency. Compression oscillations can be seen in Fig. 7 where we plot the vertical radius of the released condensate as a function of hold time t_h in the trap. To excite the oscillation we step the scattering length from a value of $a = 363\,a_0$ ($B = 24.4$ G) to $a = 25\,a_0$ ($B = 17.6$ G) at time t_0. The condensate is then allowed to oscillate in the trap for a variable hold time t_h at the final value of the scattering length. We release the condensate at time $t_0 + t_h$ and take an image after 80 ms of free expansion. We fit the data by a sinusoidal function. The measured compression oscillation frequency of (58.3 ± 0.2) Hz agrees well with twice the radial trap frequency of $2 \times (28 \pm 1)$ Hz at the given trapping power. To account for the damping we have to introduce an exponential decay of the amplitude and of the offset value. The damping of the amplitude has a time constant of 126 ms. We have not yet identified the origin of this damping. Possibly the BEC samples different trapping frequencies due to the large amplitude of the oscillation, which would lead to an apparent damping. Also, damping might be caused by the interaction

with a residual thermal cloud or by parametric processes [38].

5 Conclusion

We have shown that essentially pure Cs condensates can be produced with more than 10^5 atoms. In our optical trap it is possible to flexibly change the atomic scattering properties. The atomic condensate can now be used as the starting point for experiments where a tuning and ramping of the scattering properties can be exploited. It will be interesting to study the case of a non-interacting condensate at the zero-crossing of the scattering length. Such a condensate might be used in atom interferometers where one wishes to suppress any mean-field effects [39]. On the other hand, tuning to large values of the scattering length might allow the investigation of effects beyond the mean-field approximation [35]. Also, modulation of the scattering length could be used as an alternative tool to probe the excitation spectrum of the condensate. Finally, ultracold Cs_2 molecules can be created by ramping across one of the Feshbach resonances [8] and the transition from an atomic to a molecular condensate could then be studied.

Acknowledgements This work is supported by the Austrian "Fonds zur Förderung der wissenschaftlichen Forschung" (FWF) within SFB 15 (project part 16) and by the European Union in the frame of the Cold Molecules TMR Network under Contract No. HPRN-CT-2002-00290. M.M. is supported by DOC [Doktorandenprogramm der Österreichischen Akademie der Wissenschaften]. C.C. is supported by a Lise-Meitner-Fellowship from the FWF.

References

1. M. Barrett, J. Sauer, M. Chapman: Phys. Rev. Lett. **87**, 010404 (2001)
2. Y. Takasu, K. Maki, K. Komori, T. Takano, K. Honda, M. Kumakura, T. Yabuzaki, Y. Takahashi: Phys. Rev. Lett. **91**, 040404 (2003)
3. G. Cennini, G. Ritt, C. Geckeler, M. Weitz: Phys. Rev. Lett. **91**, 240408 (2003)
4. T. Weber, J. Herbig, M. Mark, H.-C. Nägerl, R. Grimm: Science **299**, 232 (2003)
5. D. Rychtarik, B. Engeser, H.-C. Nägerl, R. Grimm: Phys. Rev. Lett. **92**, 173003 (2004)
6. C. Chin, A. J. Kerman, V. Vuletic, S. Chu: Phys. Rev. Lett. **90**, 033201 (2003)
7. C. A. Regal, C. Ticknor, J. L. Bohn, D. S. Jin: Nature **424**, 47 (2003)
8. J. Herbig, T. Kraemer, M. Mark, T. Weber, C. Chin, H.-C. Nägerl, R. Grimm: Science **301**, 1510 (2003)
9. S. Dürr, T. Volz, A. Marte, G. Rempe: Phys. Rev. Lett. **92**, 020406 (2004)
10. K. Xu, T. Mukaiyama, J. R. Abo-Shaeer, J. K. Chin, D. E. Miller, W. Ketterle: Phys. Rev. Lett. **91**, 210402 (2003)
11. S. Jochim, M. Bartenstein, A. Altmeyer, G. Hendl, S. Riedl, C. Chin, J. Hecker Denschlag, R. Grimm: Science **302**, 2101 (2003)
12. M. Greiner, C. A. Regal, D. S. Jin: Nature **426**, 537 (2003)
13. C. Chin, V. Vuletic, A. J. Kerman, S. Chu, E. Tiesinga, P. J. Leo, C. J. Williams: Phys. Rev. A to appear
14. E. A. Donley, N. R. Claussen, S. T. Thomson, C. E. Wieman: Nature **417**, 529 (2002)
15. L. Radzihovsky, J. Park, P. B. Weichman: Phys. Rev. Lett. **92**, 160402 (2004)
16. M. W. J. Romans, R. A. Duine, S. Sachdev, H. T. C. Stoof: Phys. Rev. Lett. **93**, 020405 (2004)
17. J. Söding, D. Guéry-Odelin, P. Desbiolles, G. Ferrari, J. Dalibard: Phys. Rev. Lett. **80**, 1869 (1998)
18. J. Arlt, P. Bance, S. Hopkins, J. Martin, S. Webster, A. Wilson, K. Zetie, C. J. Foot: J. Phys. B **31**, L321 (1998)
19. D. Guéry-Odelin, J. Söding, P. Desbiolles, J. Dalibard: Europhys. Lett. **44**, 26 (1998)
20. D. Guéry-Odelin, J. Söding, P. Desbiolles, J. Dalibard: Optics Express **2**, 323 (1998)
21. S. A. Hopkins, S. Webster, J. Arlt, P. Bance, S. Cornish, O. Maragò, C. J. Foot: Phys. Rev. A. **61**, 032707 (2000)
22. P. J. Leo, E. Tiesinga, P. S. Julienne, D. K. Walter, S. Kadlecek, T. G. Walker: Phys. Rev. Lett. **81**, 1389 (1998)
23. A. M. Thomas, S. Hopkins, S. L. Cornish, C. J. Foot: J. Opt. B **5**, S107 (2003)
24. H. Perrin, A. Kuhn, I. Bouchoule, C. Salomon: Europhys. Lett. **42**, 395 (1998)
25. V. Vuletić, A. J. Kerman, C. Chin, S. Chu: Phys. Rev. Lett. **82**, 1406 (1999)
26. M. Hammes, D. Rychtarik, V. Druzhinina, U. Moslener, I. Manek-Hönninger, R. Grimm: J. Mod. Opt. **47**, 2755 (2000)
27. D.-J. Han, M. T. DePue, D. S. Weiss: Phys. Rev. A **63**, 023405 (2001)
28. T. Weber, J. Herbig, M. Mark, H.-C. Nägerl, R. Grimm: Phys. Rev. Lett. **91**, 123201 (2003)
29. D. J. Han, Marshall T. DePue, David S. Weiss: Phys. Rev. A **63**, 023405 (2001)
30. A. J. Kerman, V. Vuletić, C. Chin, S. Chu: Phys. Rev. Lett. **84**, 439 (2000)
31. D. M. Stamper-Kurn, H.-J. Miesner, A. P. Chikkatur, S. Inouye, J. Stenger, W. Ketterle: Phys. Rev. Lett. **81**, 2194 (1998)
32. T. Weber: PhD thesis, Univ. Innsbruck 2003
33. P. Treutlein, K. Y. Chung, S. Chu: Phys. Rev. A **63**, 051401 (2001)
34. W. Ketterle, N. J. Van Druten: Adv. At. Mol. Opt. Phys. **37**, 181 (1996)
35. L. Pitaevskii, S. Stringari: *Bose-Einstein Condensation* (Clarendon Press, Oxford 2003)
36. S. L. Cornish, N. R. Claussen, J. L. Roberts, E. A. Cornell, C. E. Wieman: Phys. Rev. Lett. **85**, 1795 (2000)
37. Y. Kagan, E. L. Surkov, G. V. Shlyapnikov: Phys. Rev. Lett. **79**, 2604 (2001)
38. F. Chevy, V. Bretin, P. Rosenbusch, K. W. Madison, J. Dalibard: Phys. Rev. Lett. **88**, 250402 (2002)
39. S. Gupta, K. Dieckmann, Z. Hadzibabic, D. E. Pritchard: Phys. Rev. Lett. **89**, 140401 (2002)